ADVANCED FUNCTIONAL MATERIALS
www.afm-journal.de

Materials Views
www.MaterialsViews.com

Photostimulated Au Nanoheaters in Polymer and Biological Media: Characterization of Mechanical Destruction and Boiling

*Dominik Hühn, Alexander Govorov, Pilar Rivera Gil, and Wolfgang J. Parak**

Agglomerated gold nanoparticle clusters embedded in polyelectrolyte films are optically excited, which results in local ablation of material from the polyelectrolyte films and in some cases leads to the formation of a gas bubble. Evidence is given that this process is mediated by superheating of the medium around the excited gold nanoparticle clusters. This process is highly dependent on the medium used. Besides the boiling point, salt and proteins in the medium also affect the formation of gas bubbles. These data demonstrate that the type of medium must be considered when describing light-mediated heating of gold nanoparticle clusters, which are fixed in a matrix surrounded by medium.

1. Introduction

Gold nanoparticles (Au NPs) hold great promise for biological applications.[1–4] This promise goes back to the fact that they present a strong absorption band in the visible to NIR region, which is the origin of the observed red to purple colors of gold NPs in solution. This absorption band results from the collective oscillation of the conduction-band electrons (the so-called electron gas) in resonance with the frequency of the incident electromagnetic field and is known as surface plasmon resonance (SPR) absorption. The influence of shape and interparticle distance is, in general, even greater than that of size. While a single absorption band is present for spherically symmetric gold NPs, multiple absorption bands correlated with their various axes appear for nonspherical ones; this is the case for gold nanorods which possess two different resonance modes due to electron oscillation across and along the long axis of the nanorod that are commonly labelled the transverse and longitudinal modes.[5] Of special relevance is the tuning of the SPR absorption through the modulation of the distance between neighboring NPs, which is usually afforded by means of encapsulation with an insulating layer, made, for example, of silica or organic capping agents.[6–8] In this fashion the interparticle spacer can screen the dipole–dipole interparticle interactions in such a way that the collective optical properties can be modulated between those of the bulk metal and those of individual NPs. Upon optical excitation at the SPR frequency significant amounts of energy can be pumped into the conduction electrons. Electron lattice coupling results in transfer of this energy from the electrons to the crystal lattice,[9–12] from where it is dissipated as heat to the local environment.[11,13–15] In this way gold NPs can be considered as a light-controlled nano-oven.[10,16] Photogenerated local heat has been used, for example, to directly destroy local tissue,[17–20] to melt matrices and thus open containers to release molecules to the local environment,[21–26] to break molecular bonds,[27–29] and to weld tissue.[30] Arguably biological applications of photoinduced heating take place in biological environments,[31] which involves the presence of salts, proteins, etc. While the processes of photoinduced heating have been investigated in detail concerning absorption,[32–34] relaxation of the excited electron gas,[35] and dissipation to basic continua such as water or ice,[10,36–38] the influence of the composition of the surrounding medium has not been fully elucidated to date because of the complexity of interactions between inorganic elements (e.g., Au NPs) and biological systems.[17] The understanding of nanostructure–biosystem interactions is especially important since the potential and current use of Au NP heaters implies thermal and physical contact of NPs with biological media such as tissue, blood, etc. In the present study we investigated the influence of the composition of the fluidic media, including biological fluids (serum, growth medium, etc.), around Au NPs on light-induced heating of polymer matrices. For this purpose agglomerates of Au NPs were embedded in polymer films created by layer-by-layer (LbL) assembly.[39] Layers were locally destroyed by photoinduced heating of the embedded Au NPs. Hereby the influence of the composition of the aqueous solution above and within the polymer films was investigated.

D. Hühn, Dr. P. Rivera Gil, Prof. W. J. Parak
Fachbereich Physik and WZMW
Philipps-Universität Marburg
Renthof 7, 35032 Marburg, Germany
E-mail: wolfgang.parak@physik.uni-marburg.de
Prof. A. Govorov
Department of Physics and Astronomy
Ohio University
Athens, Ohio 45701, USA

DOI: 10.1002/adfm.201101134

2. Strategy and Theoretical Expectations

2.1. Materials

Poly(allylamine hydrolchloride) (PAH; ref 283223, M_w = 56 kDa), poly(fluorescein isothiocyanate allylamine hydrochloride) (PAH_{FITC}, ref 630209, M_w = 56 kDa, ratio PAH:FITC

50:1), poly(sodium 4-styrenesulfonate) (PSS, ref 243051, M_w = 70 kDa), albumin from bovine serum (BSA, ref A9647, M_w = 66 kDa), albumin–fluorescein isothiocyanate conjugate (BSA_{FITC}, ref A9771, M_w = 66 kDa, ratio FITC:BSA 7:1), glycerol (ref G8773), minimum essential medium eagle (basal medium, ref M4655), and penicillin–streptomycin (ref P4333) were purchased from Sigma-Aldrich (Germany). The polyelectrolytes PAH (or PAH_{FITC}) and PSS were dissolved in 0.5 M NaCl solution. The concentration of PAH or PAH_{FITC} was 1.872 mg mL^{-1} and the concentration of PSS was 4.124 mg mL^{-1}, to give an equal number of charged groups present in solution. After dissolution the pH was adjusted to 6.5 by addition of HCl or NaOH. BSA_{FITC} was dissolved in pure water with a concentration of 0.5 mg mL^{-1}. Growth medium for cell culture was made by combination of basal medium with 10% fetal bovine serum (serum, ref S 0615, Biochrom), 1% penicillin–streptomycin, and 1% L-glutamine (ref 25030-024, Invitrogen). Lime-soda-glass slides (ref H868.1), NaCl (cellpure, ref HN00.2), methanol (ref 8388.5), ethanol (ref T171.2), 2-propanol (ref 7343.1), toluene (ref 9558.3), *N*,*N*-dimethylformamide (DMF, ref 6251.2), and monoethylene glycol (MEG, ref 6881.2) were purchased from Roth. Au NPs (15 nm core diameter, citrate-coated, ref EMGC15) were purchased from British Biocell International. All solutions were based on three-stage purified water (R = 18.2 MΩ·cm at 25 °C, Milli-Q Academic, Millipore).

2.2. Sample Preparation and Characterization

Multilayered thin films on glass slides were prepared by the LbL deposition technique.[40] Glass slides were cleaned first by sonication for 30 minutes at 60 °C in a water/ethanol mixture (3:7) with 1% KOH, and then subsequently washed exhaustively with pure water. This procedure ensured negatively charged surfaces. For polymer films without proteins the pretreated glass slides were dipped for 5 minutes into PAH_{FITC} solution, which resulted in attachment of PAH_{FITC} to the surface and inversion of the surface charge. The glass slides were then subsequently dipped for 5 minutes into PSS solution, whereupon PSS adsorbed and restored the original charge. After each immersion an intermediate washing step was performed to remove unbound material. Upon repetition of the PAH and PSS adsorption steps, processed multilayers with the architecture $(PAH_{FITC}/PSS)_n$ were grown. To embed BSA_{FITC} into the polymer film, the LbL procedure was applied as described above. However instead of PAH_{FITC} unlabeled PAH solution was used. BSA_{FITC} was added as an intermediate layer between PAH and PSS by incubation of the PAH terminated surface with 1 ml of the BSA_{FITC} solution. Due to the negative charge of BSA (isoelectric point: 4.7) at neutral pH the proteins adsorb onto the positively charged surface. PSS is believed to stabilize layer growth by completing the negatively charged layer. This procedure led to the architecture $(PAH/BSA_{FITC}+PSS)_n$. To embed aggregated Au NP clusters the procedure was repeated as for embedding of BSA, substituting aggregated Au NP clusters for BSA. For this purpose the Au NPs first had to be aggregated. Au NPs (c ≈ 2 nM in water) were mixed with the same volume of 0.5 M NaCl. As soon as the NaCl solution had been added the Au NPs started to aggregate (color changed from red to bluish) and the solutions had to be used for integration into the polyelectrolyte layers within several minutes, whereby the incubation time depended on the desired grade of aggregation. It is believed that Au clusters still carry enough charge to be adsorbed onto the PAH terminated layer even though they become agglomerated by screening of charged citrate molecules. In addition to electrostatic attraction, van der Waals attraction in close proximity to the surface might enhance stable incorporation of Au NP clusters.[41] Samples with incorporated Au NPs finally consisted of three layers of Au NP clusters and ten layers of BSA_{FITC} in-between PAH and PSS. As the same Au solution was taken for all three layers, different sizes of clusters were embedded (the Au NP agglomerates still were growing while the subsequent layers were assembled). Thus, the final architecture of these samples was $(PAH/Au+PSS)_3(PAH/BSA_{FITC}+PSS)_{10}$. Multilayer growth of polyelectrolyte films was quantified by fluorescence measurements using a Fluorolog FL3-22 from Horiba Jobin Yvon (excitation wavelength: 495 nm) equipped with a solid sample holder with fine angle adjustment on dried samples. Hereby addition of each fluorescent layer (PAH_{FITC} or BSA_{FITC}) of the fluorescent samples $(PAH_{FITC}/PSS)_n$, $(PAH/BSA_{FITC}+PSS)_n$, $(PAH/Au/PSS)_3(PAH/BSA_{FITC}+PSS)_{10}$ was observed after every PSS step. After preparation all samples were stored in Rotilabo®-slide tubes (ref KL89.1) from Roth at 4 °C. Before measurements, samples were dried in a nitrogen stream.

2.3. Microscope Set-Up

Light irradiation experiments on the polyelectrolyte samples were carried out with a microscope set-up consisting of an upright Axiotech microscope from Zeiss (Germany) equipped with an additional continuous wave near-infrared (NIR) laser diode emitting at 830 nm. The NIR laser beam was coupled into the microscope using a beam splitter (2P-Strahlenteiler 725 DCSPXR, ref F33-725, AHF Analysentechnik) and was focused by changing the working distance with an *x*–*y* stage (**Figure 1**). The polyelectrolyte samples were placed on a micrometer-resolution motorized *x*–*y*–*z* stage (SMI, Luigs & Neuman Feinmechanik und Elektrotechnik GmbH, Germany) in the focus of the microscope. As microscope imaging was operated in reflection, small silicon wafers served as the mirror below the polyelectrolyte sample. The microscope was furthermore equipped with several filters. Transmission, green fluorescence (Filtersatz 09, excitation BP 450–490, beam splitter FT 515, emission LP 515, ref 488009-9901-000, Zeiss Germany), and red fluorescence (Filtersatz 00, excitation BP 530–585, beam splitter FT 600, emission LP 615, ref 488000-0000-000, Zeiss Germany) were investigated. Filters were mounted into a filter bar that had to be shifted manually. In transmission mode a 100 W white-light halogen lamp (HAL-100, Zeiss Germany) served as the light source. For fluorescence observations a mercury-vapor lamp (HBO-100, Zeiss Germany) was used. The light beam for transmission and fluorescence illumination and the NIR laser beam for the excitation of the Au NPs were focused onto the polyelectrolyte sample with a water immersion objective (W Plan-Apochromat 63x/1.0 Ph3, ref 441471-9910-000, Zeiss Germany). Images were recorded with a charge-coupled device (CCD) true-color camera (MRc AxioCam,

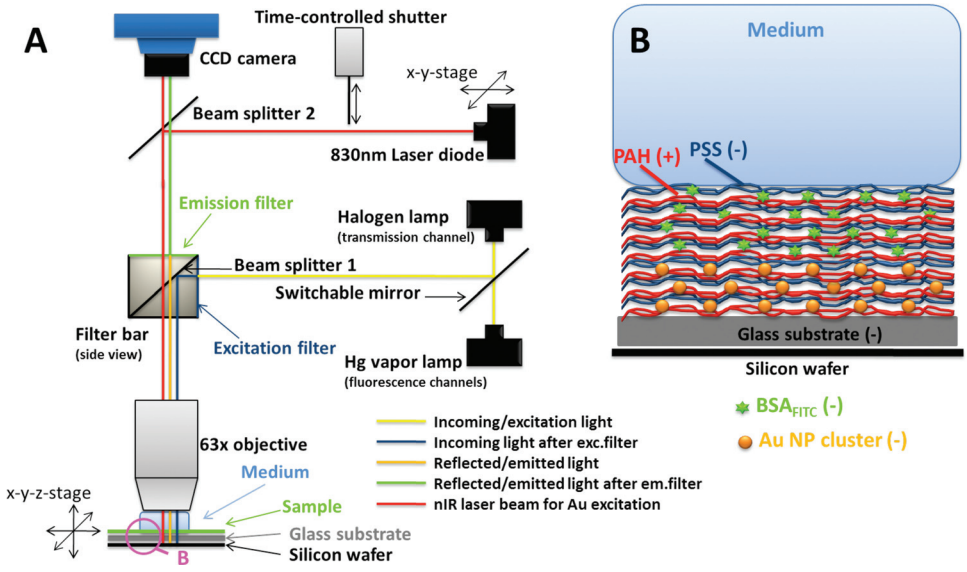

Figure 1. Experimental set-up. A) An 830 nm NIR laser is coupled into an inverted microscope via beam splitter #2. In parallel the illumination for transmission or fluorescence is coupled with beam splitter #1. In this way a laser spot of a few micrometers can be generated on a sample in the focus of a 63x objective (cf. Figure 2), as well as illuminating the sample in the viewing area of the objective. Light reflected from or originating from fluorescence of the sample is imaged after having passed appropriate filters with a CCD camera. B) The sample consists of Au NP clusters embedded in a polymer film which has been assembled by LbL deposition on a glass slide, placed on top of a silicon wafer, which acts as mirror. As the thickness of one polyelectrolyte layer is around 1 nm[51] and the diameter of one Au NP cluster is 0.1–10 µm; the scheme is not drawn to scale. The sample is immersed in medium, which is varied within this work between different buffers.

Zeiss Germany) and further analyzed with the AxioVision software (Rel. 4.6, Zeiss Germany). Part of the NIR laser light was absorbed by the optical components of the microscope set-up. Therefore the laser intensity in the focal plane was determined with a power meter (PM100 display unit with S130A slim sensor, Thorlabs). The NIR laser was completed with a self-constructed shutter system, which allowed control over the excitation of the polyelectrolyte samples. For NIR excitation of the sample a 150 µL drop of medium solution was put on top of the dried polyelectrolyte films. The lens of the water objective immersed this drop and the distance in-between sample and lens was adjusted until the sample was focused. The NIR laser spot was aimed at single Au clusters in the polyelectrolyte samples, which were then exposed by opening the shutter for 1 second (**Figure 2**). Transmission and fluorescence images of the polyelectrolyte layers were taken before and after NIR exposure. Upon NIR exposure of the $(PAH/Au+PSS)_3(PAH/BSA_{FITC}+PSS)_{10}$ samples, part of the polyelectrolyte layers around the excited Au NP cluster had been removed, which appeared as black hole in the green fluorescence channel, and a gas bubble had formed (**Figure 3**). For each experiment the cross-sectional area $A_{cluster}$ of the excited Au NP cluster before excitation, the area of the resulting hole in the polyelectrolyte film $A_{hole,}$ and the cross-section A_{bubble} of the gas bubble after excitation were determined from the recorded transmission and fluorescence images (**Figure 4**). For different experiments the laser power P_{laser} and the medium on top of the polyelectrolyte film were varied.

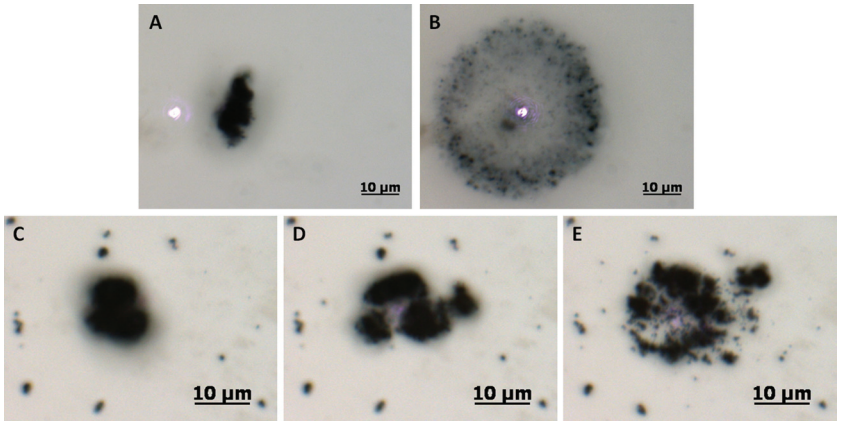

Figure 2. Mechanical disintegration of Au NP clusters upon NIR illumination. A) Illumination of a site next to an Au NP cluster leads to no effect. B) When the NIR laser spot (P_{laser} = 10 mW) is aimed at the same Au NP cluster as in (A) the cluster disintegrates mechanically and the Au NPs are spread upon switching on the laser. C–E) In the case of lower laser powers (P_{laser} = 4 mW) illumination of the cluster causes fragmentation of the cluster instead of complete disintegration.

2.4. Boiling Point, Surface Tension, and Viscosity Measurements

Basic properties of the medium above the polyelectrolyte film such as boiling point, surface tension, and viscosity were determined.

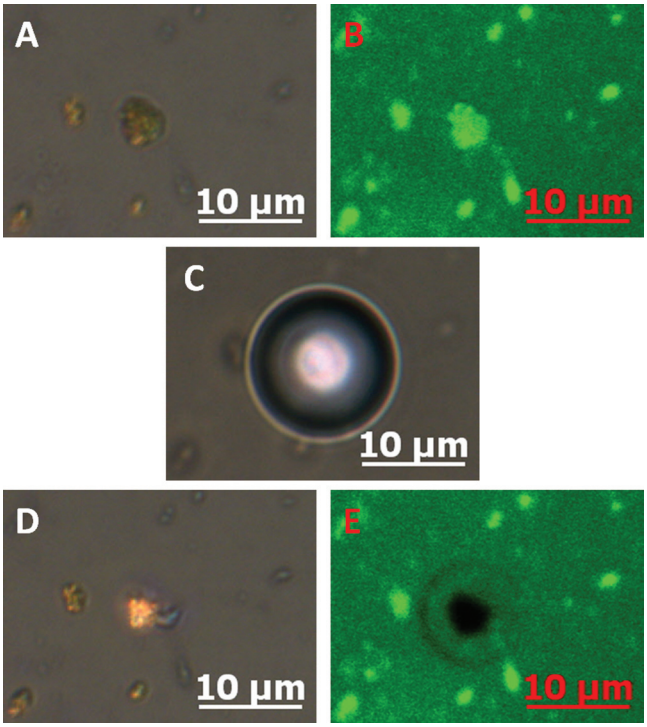

Figure 3. A polyelectrolyte film with integrated Au NP clusters (geometry $(PAH/Au+PSS)_3(PAH/BSA_{FITC}+PSS)_{10}$) is shown in A) phase-contrast and B) fluorescence mode as imaged with the objective as in the microscopy set-up shown in Figure 1. Au NP clusters appear brighter compared to the background in the phase-contrast image. The fluorescence originates from the BSA_{FITC} which is integrated into the polymer film. C) Upon excitation for 1 s a vapor bubble appears, which is shown directly after the shutter is closed, where the bubble reached its maximum cross-sectional area. After the bubble has disappeared a hole remains in the polymer film around the excited Au NP cluster, as can be seen in D) phase-contrast and E) fluorescence images. The phase-contrast image suggests that part of the Au NP cluster remain at the original position, whereas the fluorescence image demonstrates that the polyelectrolyte film including the incorporated BSA has been locally removed.

For determination of the boiling point, media were heated on a hot plate while measuring the equilibrated temperature when boiling. In the cases of serum and growth medium a boiling point could not be determined as coagulation occurred before an equilibrated temperature was reached. The surface tension was measured by pulling an aluminum ring, wetted in a sufficient amount of medium, out of the medium.[42] Thereupon a nearly cylindrical thin film of medium was formed in-between the ring and the medium surface. From the applied force at the point where the film collapsed, the surface tension could be calculated. The viscosity was measured following the law of Hagen–Poiseuille.[42] A fixed amount of medium was stored in a reservoir, from where it could run vertically downwards through a thin glass capillary into a collection beaker. From the time until the medium had completely passed through the capillary and the comparison of surface levels in the reservoir and the collection beaker before and after the flow, the viscosity could be calculated.

2.5. Theoretical Modeling

In **Figure 5** we have depicted a simple model to estimate the temperature in our system. First of all, we notice that the laser-beam diameter ($d_{beam} \approx$ µm) is smaller than the typical diameter of Au NP aggregates (≈few µm). For further estimates, we will assume the Au NP cluster diameter to be $d_{cluster}$ = 3–8 µm. A cluster effective dielectric function (ε_{eff}) can be written using the Maxwell–Garnett equation:[43]

$$\varepsilon_{eff} = \varepsilon_0 \frac{\varepsilon_{NP}(1+2\alpha) - \varepsilon_0(2\alpha - 2)}{\varepsilon_0(2+\alpha) + \varepsilon_{NP}(1-\alpha)} \quad (1)$$

where ε_{NP} and ε_0 are the dielectric functions of metal (the Au NPs) and voids. Voids are filled mostly with surfactant molecules (the citrate capping around the Au NPs) and we assume that $\varepsilon_0 = 2$ (polymer); ε_{NP} is taken for Au from the tables.[44] In Equation (1), α is a filling factor that will be taken as 0.43 (Au NP spheres have ca. 1 nm surface-to-surface distance due to the citrate capping on the NP surface, which acts as spacer). Since $d_{beam} < d_{cluster}$, an approach of geometric optics can be employed for estimates. Using the above effective dielectric function, we see that clusters with $d_{cluster}$ = 3–8 µm are not transparent to the beam. At an excitation wavelength of 830 nm, the decay length for the light penetrating the effective medium is ≈2 µm. Assuming that the laser beam strikes a flat surface of an effective material (Au NPs and voids), the power absorbed by the cluster will be given by Equation 2:

$$P_{absorbed} = P_{laser} \cdot (1 - R) \quad (2)$$

where P_{laser} is the incident laser power, $R = |\sqrt{\varepsilon_{eff}} - \sqrt{\varepsilon_{med}}|^2 / |\sqrt{\varepsilon_{eff}} + \sqrt{\varepsilon_{med}}|^2$ is the reflection coefficient, and ε_{med} is a dielectric constant of a medium (Figure 5). Using the above effective-medium approach and taking ε_{med} = 1.8–2 (water, polymer, or a biological medium), we see that the absorption of light by the cluster is very efficient: $A = (1 - R) \approx 0.95$. Now we look at the thermal part of the problem. A heated cluster is located on a boundary of two media, fluid medium above and glass below (Figure 5). By assuming that the cluster of Au NPs is spherical and located at the boundary of the two media, we write an estimate (Equation 3) for the temperature at the outer surface of a spherical cluster under steady illumination:[13]

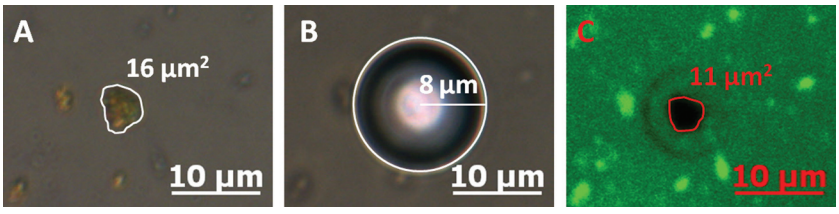

Figure 4. From the experimental observations shown in Figure 3 the following parameters are extracted. A) The cross-sectional area $A_{cluster}$ of the excited Au NP cluster before excitation. B) The cross-section A_{bubble} of the gas bubble immediately after excitation, derived from the radius r_{bubble} with $A_{bubble} = \pi \cdot r_{bubble}^2$, and C) the area of the resulting hole in the polyelectrolyte film A_{hole}.

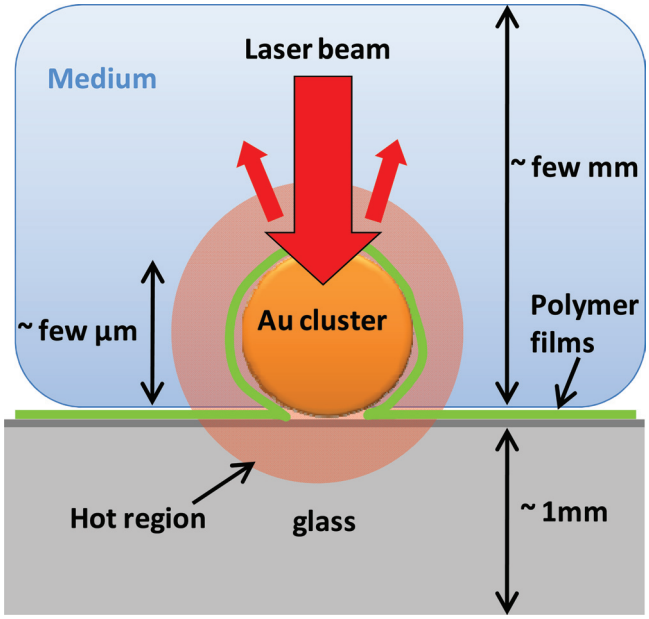

Figure 5. Geometry used for the theoretical modeling.

$$T = T_{\text{room}} + \Delta T \approx T_{\text{room}} + \frac{P_{\text{absorbed}}}{2\pi k_{\text{av}} d_{\text{cluster}}} = T_{\text{room}} + \frac{P_{\text{laser}}\ (1 - R)}{2\pi k_{\text{av}} d_{\text{cluster}}} \tag{3}$$

where $k_{\text{av}} = (k_{\text{glass}} + k_{\text{med}})/2$ is an averaged thermal conductivity of the neighboring media. Typical numbers for thermal materials parameters are the following: $k_{\text{glass}} \approx 1$ W mk^{-1} and $k_{\text{med}} \approx k_{\text{water}} = 0.6$ W mk^{-1}. We note that the above approximation for k_{med} is quite reliable for many biological media.[45] Then, we obtain the following numerical result (Equation 4) for the temperature at the outer surface of the Au NP cluster:

$$T = 20\,^{\circ}\text{C} + 189\,^{\circ}\text{C}\frac{P_{\text{laser [mW]}}}{d_{\text{cluster [µm]}}} \tag{4}$$

where P_{laser} [mW] is the incident power in mW and d_{cluster} [µm] is the diameter of an Au NP cluster in µm.

3. Results and Discussion

3.1. Mechanical Manipulation of Au NP Clusters upon Excitation

Optical excitation of Au NPs leads to heating of the particles and imposes momentum by means of an optical force.[41,46,47] Hereby resonant and off-resonant excitation has to be distinguished. As we used Au NP clusters instead of single Au NPs in the present study, a sharp plasmon resonance frequency as present for single particles no longer existed. Due to the broad absorption band[48] which also contains the applied laser wavelength, both effects (heat generation and translational motion) have to be considered as being responsible for the following effects. In Figure 2 excitation of one Au NP cluster (without being embedded in a polyelectrolyte film) is demonstrated. Note that NIR excitation was at 830 nm, whereas the surface plasmon resonance of individual Au NPs (diameter: 15 nm) is at 520 nm. Light is absorbed only due to the fact that the Au NPs have been aggregated into clusters (Figure SI.4, Supporting Information). As can be seen in Figure 2 the excitation of Au NP clusters led to a mechanical explosion of the clusters. This effect depended on the excitation power P_{laser}. Mechanical disintegration of clusters was observed at rather high powers (ca. 10 mW). For lower powers (≤4 mW) this effect decreased. Instead of complete disintegration, clusters were rather split into fragments. No effect was typically observed for powers smaller than 2 mW or when the laser was applied to a site where no cluster was present.

3.2. Local Disintegration of Polyelectrolyte Films upon Heating of Embedded Au NP Clusters

Optical excitation of Au NP clusters immobilized in polyelectrolyte films caused local destruction of the polyelectrolyte films mediated by disintegration/fragmentaion of the Au NP clusters, see Figure 3. In the following all experiments refer to the geometry $(\text{PAH/Au+PSS})_3(\text{PAH/BSA}_{\text{FITC}}\text{+PSS})_{10}$ of the polyelectrolyte multilayers. Optical excitation of an Au NP cluster with water as medium on top of the polyelectrolyte film caused the formation of a vapor bubble which stayed localized at the cluster site and decreased with time, as well as creating a remaining black hole in the green fluorescent polymer film around the heated cluster. For other media these observations could be different as, for example, in the case of using growth medium or serum on top of the polyelectrolyte film, when almost no bubbles could be observed. In Figure 4 the three parameters which were extracted out of each excitation experiment are depicted: The cross-sectional area A_{cluster} of the Au NP cluster before it had been excited, the cross-section A_{bubble} of the gas bubble which had been formed during excitation, and the area A_{hole} of the resulting hole in the fluorescent polyelectrolyte film. It has to be pointed out that quantification of these experimental parameters was not always straightforward. Only spherical objects were interpreted as a bubble whereas non-spherical moving structures at the border of a cluster during an excitation might have been caused by mechanical interference of debris of the locally destroyed polyelectrolyte film. Heating of Au NP clusters is a cooperative effect and generated heat strongly depends on the cluster size.[16] The bigger the Au NP cluster the more thermal energy is locally produced,; this induces bigger bubbles and holes in the poylmer film. We thus normalized the cross-section of the bubbles and the size of the hole in the polymer film to the size of the excited Au NP cluster: $A_{\text{bubble}}/A_{\text{cluster}}$, $A_{\text{hole}}/A_{\text{cluster}}$. Phenomenological data show that the polyelectrolyte films were efficiently effected by optical excitation of the integrated Au NP clusters. The shape of the disturbed area, i.e., the hole in the polymer film, was mostly determined by the shape of the Au NP cluster before excitation. An often-seen phenomenon was the formation of a green border of greater fluorescence around the black hole after excitation, which indicated that film material had been mechanically pushed away (Figure SI.13, Supporting Information). In many other cases the black hole was surrounded by another ring of

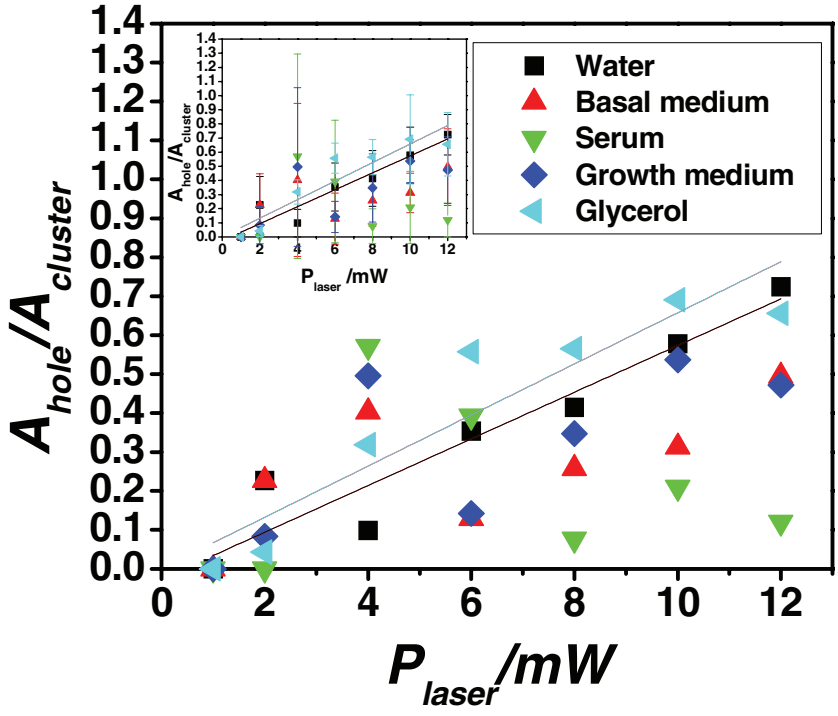

Figure 6. A_{hole}, normalized to $A_{cluster}$, is plotted P_{laser} which had been focused to the Au NP cluster for 1 s for excitation of the Au NPs, cf. Figure 4. Experiments were performed with different media on top of the polyelectrolyte films: water, basal medium, serum, growth medium, and glycerol. The linear fits serve as guides to the eye indicating the trend observed for water and glycerol. Error bars are shown in the inset.

lower fluorescence (Figure 3E). We can only estimate that this ring originates from the boundary of a vapor bubble at the polyelectrolyte surface. Controls made by optically exciting areas of the polymer films in which no Au NP cluster was found did not result in the formation of a hole in the film and no bubbles could be observed. Therefore the effects are related to the presence of Au NP clusters and we can exclude that the black holes originated from bleaching of the FITC in the polymer film. The size of the hole depended on the laser power. In the case of water on top of the polyelectrolyte film it was found that the black hole area as well as the bubble cross-section increased almost linearly with the applied laser power, except for at lower powers ($P_{laser} \leq 4$ mW). Films might be destroyed either by melting of the polyelectrolytes, by mechanical force imposed by the disintegrating expanding Au NP clusters, or by mechanical stress upon the bubble formation, which will be discussed in more detail later on.

3.3. Analysis of the Creation of a Hole in the Polymer Film at Locations of Optically Excited Au NP Clusters

In the following an excitation series with water, basal medium, serum, growth medium, and glycerol as medium on top of the polymer film is discussed. The area of the black hole (normalized to the Au NP cluster size) $A_{hole}/A_{cluster}$ as created at the illuminated Au NP cluster (1 s excitation) is plotted versus P_{laser} (Figure 4 and **Figure 6**). As the borders of the black holes were barely visible at low illumination powers and for the glycerol- and serum-containing media, experiments were repeated several times to get meaningful mean values. For water and glycerol a clear trend towards bigger holes upon increasing laser power can be observed. In the case of glycerol the borders around the black hole in the polymer film appeared in bright green in the fluorescence channel, which indicates the presence of BSA_{FITC}-labeled polymer material originating from the area from which the polymer had been removed. In the other media (basal medium, growth medium, serum) no direct correlation between the size of the hole in the polymer film and the laser power was obvious.

3.4. Analysis of the Creation of a Bubble Adjacent to Optically Excited Au NP Clusters

In the case of water, excitation of an Au NP cluster with laser powers above 4 mW always resulted in the formation of a bubble adjacent to the cluster. This formation was also observed with water which had been degassed prior to experiments. In the case of basal medium only in some cases bubbles appeared, which resulted in a smaller mean bubble size (the mean value also comprises the results in which no bubble had formed, i.e., with bubble size 0). Within the standard deviation for water and basal medium one can conclude that an almost constant bubble size was present for various laser powers (6–12 mW) (**Figure 7**A). For lower laser powers below 4 mW the bubble size decreased rapidly to zero. Considering the probability n_{bubble} with which bubbles appeared upon illumination (Figure 7B) one can describe the result for water as "all-or-nothing-response" with a threshold of around 4 mW, as for powers above 4 mW a bubble arose during each excitation ($n_{bubble} = 1$), whereas at 2 mW no more bubbles could be observed ($n_{bubble} = 0$). For basal medium a bubble probability of ca. 20% was found between 4 mW and 12 mW. For the rest of the media no bubbles were created upon excitation of the Au NP clusters (Figure 7B). As basal medium contains around 150 mM of various salts (mainly NaCl) we speculated that differences in bubble appearance upon excitation of Au NP clusters might be influenced by ion concentration in the medium. Presence of ions screens the negative charges on the surface of Au NPs and of the polyelectrolytes which could change the geometry in the Au NP clusters (such as the average Au NP–Au NP distance). For this purpose a series of excitation of polymer films with Au NP clusters with water with variable NaCl concentration in the medium was performed (Figure 7C). Clearly the average bubble size decreased upon increasing NaCl concentration. At $P_{laser} = 12$ mW no bubbles could be observed anymore when the NaCl concentration has been increased to 1 M. However, the concentration of various salts (mainly NaCl) in

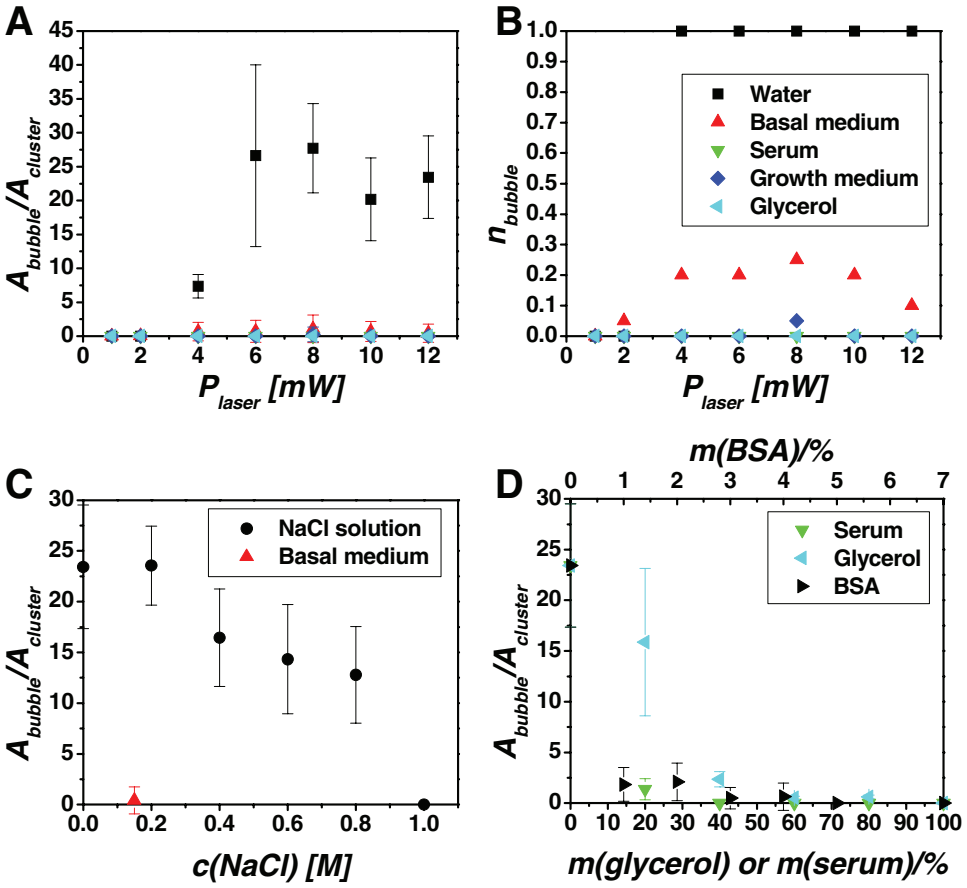

Figure 7. A) A_{bubble}, normalized to $A_{cluster}$, is plotted versus P_{laser}, which had been focused to the Au NP cluster for 1 s for excitation of the Au NPs, cf. Figure 4. Data points correspond to the same experiments as reported in Figure 6. Experiments were performed with different media on top of the polyelectrolyte films: water, basal medium, serum, growth medium, and glycerol (legend is the same as in (B)). In the cases where no bubble appeared A_{bubble} was taken as zero. As in the case of basal medium only sometimes bubbles appeared (cf. (B)) the mean bubble size is much smaller than is the case with water. B) As can be seen in (A), for several media bubbles barely occurred (i.e., $A_{bubble} = 0$). For this reason in (B) n_{bubble} is plotted for different media and excitation powers. $n_{bubble} = 1$ would refer to a situation in which in each case of illumination a bubble had appeared, and $n_{bubble} = 0$ to the case where in no case of illumination any bubble had appeared. C) The same experiment as described in (A) was performed, but with NaCl solution of different concentrations c_{NaCl} on top of the polyelectrolyte film. For all excitations we used $P_{laser} = 12$ mW. As reference also basal medium (with a salt concentration of 0.15 M) was used. D) The same experiment as described in (A) was performed, but with water as medium, to which variable amounts (in percent mass) of BSA, glycerol, or serum had been added. For all excitations we used $P_{laser} = 12$ mW. Comparable contents of proteins in the medium led to comparable average bubble sizes. The axes represent the assumption that serum is composed of 7% proteins.

basal medium, where only bubbles with a small average size appear, is only 150 mM. In contrast the frequency of bubble formation in water with 150 mM NaCl is at best slightly reduced. Though basal medium also comprises some other ions besides Na^+ and Cl^- at lower concentration (also divalent ones) the data presented in Figure 7C indicate that presence of salt is not the predominant factor which hinders formation of bubbles upon optical excitation of Au NP clusters. We suppose that bubbles arise upon superheating around excited Au NP clusters, whereby the medium is heated to a temperature higher than its boiling point. For this to happen the medium has to be free of nucleation sites. In case of pure Milli-Q water nucleation sites may be rare enough, which leads the water to form a metastable "superheated" state, and finally causes an explosionlike vaporization. In media containing more "ingredients," more nucleation sites may be present to prevent superheating and thus avoid the explosive appearance of vapor bubbles. Especially in the case of serum, the content of proteins might suppress the appearance of vapor bubbles because there are sufficient nucleation sites on the one hand and locally coagulating material on the other. Therefore another excitation series was performed to verify the influence of protein content in the medium (Figure 7D). Aqueous mixtures of bovine serum albumin (BSA) and serum served as medium and the same trend could be observed considering the normalized bubble size. The axes were chosen like this as serum is supposed to be composed of 7% from proteins (100% serum $\hat{=}$ 7% BSA). When considering glycerol, which was taken as a viscous medium for comparison, one observes that increasing viscosity might not be the crucial factor for a decreased average bubble size. To further elucidate the role of the medium for bubble formation we performed similar excitation experiments with Au NP clusters in polymer films with additional media (**Figure 8**). The media were selected to allow understanding of how parameters like boiling

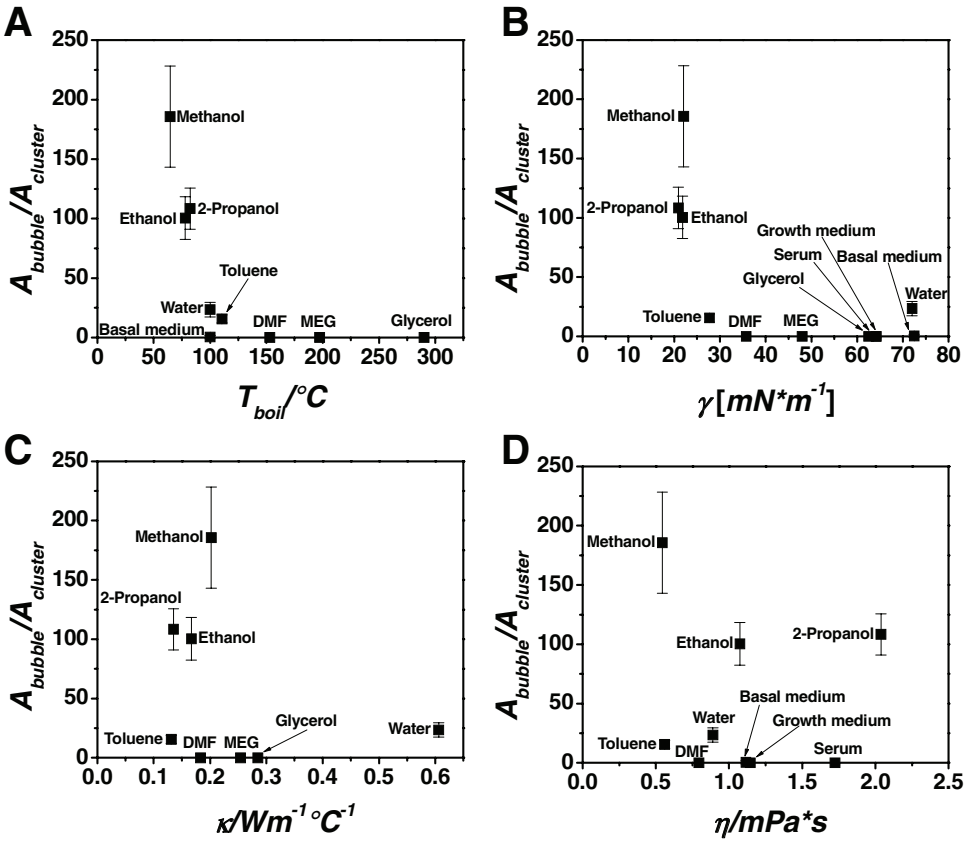

Figure 8. A_{bubble} upon laser illumination, normalized to $A_{cluster}$, is plotted versus A) T_{boil}, B) γ at 25 °C, C) κ, and D) η of different media on top of the polyelectrolyte film. Au NP clusters were hereby illuminated with $P_{laser} = 12$ mW for 1 s, cf. Figure 4. Experiments were performed with different media on top of the polyelectrolyte films: water, methanol, ethanol, 2-propanol, toluene, DMF, MEG, glycerol, basal medium, serum, and growth medium. In the case of serum and growth medium (which contains 10% serum) no boiling point could be determined, as the proteins in solution coagulated upon heating. Also the thermal conductivity was not determined for these two media. In (D) glycerol and MEG are not displayed for clarity due to their high η values.

point T_{boil}, surface tension γ, thermal conductivity κ, and viscosity η influence the formation of vapor bubbles. As supposed, superheating might be the reason for the appearance of bubbles as the dependence on the boiling point leads to a clear trend for different media with a threshold of T_{boil} between 110 °C and 150 °C (Figure 8A). No bubbles could be observed above a boiling point of 150 °C. This result, however, does not automatically mean that for these media the boiling point is not reached, as thermal energy is permanently transported away from the Au NP cluster, which may avoid local superheating. Basal medium, however, has a boiling point below the indicated threshold, so here another explanation has to be found. Indeed the impurity of media (salt and other contents) might be the crucial parameter as discussed below. In Figure 8C the dependence of bubble formation on the thermal conductivity of the medium (which is the parameter which quantifies the heat transportation capability) is plotted. κ is of the same order of magnitude (0.1 – 0.3 $W \cdot K^{-1} \cdot m^{-1}$) for all media except water. However, no clear trend can be observed in the bubble size versus thermal conductivity relation. At any rate, low thermal conductivity seems to be beneficial for local superheating if the boiling point is low enough. The dependence of the bubble size on the surface tension of the medium is shown in Figure 8B. For most media the surface tension increases almost linearly with the boiling point, which results in a comparable profile: decreasing bubble size with increasing surface tension, similar to decreasing bubble size with increasing boiling point. Water, however, does not fit in this scheme. Water has a rather high surface tension due to its high polarity and exhibits strong molecular interaction. No dependence of the bubble size on the viscosity of the medium was found (Figure 8D). This result leaves the boiling point of the medium as the most influential parameter for bubble size upon local optical excitation of Au NP clusters, but it does not, however, explain the fact that addition of salt reduces formation of bubbles as addition of salt (e.g., NaCl) leads to an increase in T_{boil} that is still below the found threshold in Figure 8A. By following Raoult's law together with the Clausius–Clapeyron equation, the extent of boiling point elevation can be calculated to be $\Delta T_{boil} \approx 6.3$ °C for a concentration of 6.14 M, which corresponds to the maximum solubility of NaCl in water. As discussed above, the addition of salt could affect the geometry of the polymer layers and the Au NP clusters. Salt could reduce the interparticle distance in the Au NP clusters, which, however, should lead to more bubbles upon increased NaCl concentration (there is more heat generation among closely spaced NPs[16]), which is in contrast to the

experimental data. Thus, as Au NPs had been agglomerated to clusters before incorporation in the polyelectrolyte films, the addition of more salt may not induce more agglomeration. However, salt may also affect the layer geometry. Salt can affect the charged sites of the layers, such that the competitive ion pairing between the oppositely charged layers and the respective counterion reduces the binding force between layers.[49] Thus permeability for molecules out of the layers could be higher when salt is present,[50] which might increase the content of nucleation sites above the LbL film. As the influence of salt still does not explain the results obtained with serum-containing media still another effect must play a role. Proteins in serum containing medium coagulate before the boiling point of the medium is reached. Coagulated proteins could act as further nucleation sites, which would thus prevent superheating and the formation of big gas bubbles.

3.5. Results of Theoretical Modeling

With Equation (4) from the theoretical model we now can estimate the cluster surface temperature for clusters with $d_{cluster}$ = 3–8 μm. We now see that the temperature achieves 100 °C for the following laser powers P_{laser}: 1.3 ($d_{cluster}$ = 3 μm) and 3.4 mW ($d_{cluster}$ = 8 μm). Active boiling of water in the experiments starts at ca. 4 mW (Figure 7). This power corresponds to ca. 114 °C ($d_{cluster}$ = 8 μm) and ca. 270 °C ($d_{cluster}$ = 3 μm). The above numbers for the temperature are greater than 100 °C which is not surprising since it is expected that the boiling process starts under the superheated conditions.[38] We therefore see that our simple model for the local temperature gives numbers that are in reasonable agreement with the experimental findings. Finally, we comment that the formation of holes in the polymer film in our experiments begins at $P_{laser} \approx 2$ mW. The above temperature estimates are actually valid for the maximum temperature outside the polymer film, at the water–polymer boundary. For a spherical heated object under steady-state conditions (i.e., under continuous illumination) the temperature outside Equation (3) is given by the total power generated ($P_{absorbed}$) and by the thermal conductivity (k_{av}) of the surrounding matrix. Note that Equation (3) does not include the thermal conductivity of the polymer film. The temperature inside the polymer and the Au NP cluster can be higher since the polymer film can create a thermal barrier for heat flow. Indeed, polymer films may have a poor thermal conductivity that will result in a strong overheating effect and in destruction of the polymer film at relatively low laser powers.

4. Conclusions

Light-induced heating of polymer-matrix-embedded Au NP clusters in complex media is influenced by several parameters. The formation of a gas bubble of evaporated medium is directly connected to the boiling point of the medium. Salt in the medium may affect the geometry of the polymer matrix leading to reduced gas-bubble sizes. Most important, complex media involving, for example, proteins also reduce formation of gas bubbles, which is speculated to be due to an increased number of nucleation sites which prevent superheating. These results are of great importance to biologically motivated release experiments. For light-triggered release of molecules from polymer films bubble suppression would be welcome as this would reduce mechanical stress. Bubble formation upon heating inside cells could, for example, kill cells.[24] We believe that experiments in this area are positively influenced by the fact that protein-containing media are present inside cells. This study thus helps to optimize the experimental conditions (for example laser power versus Au NP cluster size) for such biologically related release experiments (as, for example, drug delivery) in cells.

Supporting Information

Supporting Information is available from the Wiley Online Library or from the author.

Acknowledgements

This work was supported by the BMBF (Eranet grant Nanosyn) to WJP. The authors are grateful to Dr. Miguel A. Correa-Duarte for inspiring technical discussions.

Received: May 19, 2011
Revised: October 4, 2011
Published online: November 17, 2011

[1] C. M. Cobley, J. Y. Chen, E. C. Cho, L. V. Wang, Y. N. Xia, *Chem. Soc. Rev.* **2011**, *40*, 44.
[2] P. K. Jain, I. H. El-Sayed, M. A. El-Sayed, *Nano Today* **2007**, *2*, 18.
[3] P. K. Jain, X. Huang, I. H. El-Sayed, M. A. El-Sayad, *Plasmonics* **2007**, *2*, 107.
[4] R. A. Sperling, P. Rivera_Gil, F. Zhang, M. Zanella, W. J. Parak, *Chem. Soc. Rev.* **2008**, *37*, 1896.
[5] J. Perez-Juste, I. Pastoriza-Santos, L. M. Liz-Marzan, P. Mulvaney, *Coord. Chem. Rev.* **2005**, *249*, 1870.
[6] A. C. Templeton, J. J. Pietron, R. W. Murray, P. Mulvaney, *J. Phys. Chem. B* **2000**, *104*, 564.
[7] M. A. Correa-Duarte, N. Sobal, L. M. Liz-Marzan, M. Giersig, *Adv. Mater.* **2004**, *16*, 2179.
[8] V. Salgueirino-Maceira, F. Caruso, L. M. Liz-Marzan, *J. Phys. Chem. B* **2003**, *107*, 10990.
[9] P. K. Jain, W. Qian, M. A. El-Sayed, *J. Phys. Chem. B* **2006**, *110*, 136.
[10] A. O. Govorov, H. H. Richardson, *Nano Today* **2007**, *2*, 30.
[11] G. Baffou, R. Quidant, C. Girard, *Appl. Phys. Lett.* **2009**, *94*, 153109.
[12] J. Zhu, Z. Sun, J. J. Li, J. W. Zhao, *Eur. Phys. J. B* **2010**, *78*, 311.
[13] A. O. Govorov, W. Zhang, T. Skeini, H. Richardson, J. Lee, N. A. Kotov, *Nanoscale Res. Lett.* **2006**, *1*, 84.
[14] H. H. Richardson, Z. N. Hickman, A. O. Govorov, A. C. Thomas, W. Zhang, M. E. Kordesch, *Nano Lett.* **2006**, *6*, 783.
[15] H. H. Richardson, M. T. Carlson, P. J. Tandler, P. Hernandez, A. O. Govorov, *Nano Lett.* **2009**, *9*, 1139.
[16] C. Hrelescu, J. Stehr, M. Ringler, R. A. Sperling, W. J. Parak, T. A. Klar, J. Feldmann, *J. Phys. Chem. C* **2010**, *114*, 7401.
[17] L. R. Hirsch, R. J. Stafford, J. A. Bankson, S. R. Sershen, B. Rivera, R. E. Price, J. D. Hazle, N. J. Halas, J. L. West, *Proc. Natl. Acad. Sci. U. S. A.* **2003**, *100*, 13549.
[18] D. P. O'Neal, L. R. Hirsch, N. J. Halas, J. D. Payne, J. L. West, *Cancer Lett.* **2004**, *209*, 171.

[19] X. Huang, P. Jain, I. El-Sayed, M. El-Sayed, *Lasers in Medical Science* **2007**, *23*, 217.
[20] X. Huang, I. H. El-Sayed, W. Qian, M. A. El-Sayed, *J. Am. Chem. Soc.* **2006**, *128*, 2115.
[21] B. Radt, T. A. Smith, F. Caruso, *Adv. Mater.* **2004**, *16*, 2184.
[22] A. G. Skirtach, C. Dejugnat, D. Braun, A. S. Susha, W. J. Parak, H. Möhwald, G. B. Sukhorukov, *Nano Lett.* **2005**, *5*, 1371.
[23] A. G. Skirtach, A. M. Javier, O. Kreft, K. Köhler, A. P. Alberola, H. Möhwald, W. J. Parak, G. B. Sukhorukov, *Angew. Chem. Int. Ed.* **2006**, *45*, 4612.
[24] A. Muñoz_Javier, P. d. Pino, M. Bedard, A. G. Skirtach, D. Ho, G. Sukhorukov, C. Plank, W. J. Parak, *Langmuir* **2009**, *24*, 12517.
[25] E. V. Skorb, A. G. Skirtach, D. V. Sviridov, D. G. Shchukin, H. Mohwald, *ACS Nano* **2009**, *3*, 1753.
[26] D. V. Volodkin, N. Madaboosi, J. Blacklock, A. G. Skirtach, H. Mohwald, *Langmuir* **2009**, *25*, 14037.
[27] J. Stehr, C. Hrelescu, R. A. Sperling, G. Raschke, M. Wunderlich, A. Nichtl, D. Heindl, K. Kürzinger, W. J. Parak, T. A. Klar, J. Feldmann, *Nano Lett.* **2008**, *8*, 619.
[28] M. J. Kogan, N. G. Bastus, R. Amigo, D. Grillo-Bosch, E. Araya, A. Turiel, A. Labarta, E. Giralt, V. F. Puntes, *Nano Lett.* **2006**, *6*, 110.
[29] N. G. Bastus, M. J. Kogan, R. Amigo, D. Grillo-Bosch, E. Araya, A. Turiel, A. Labarta, E. Giralt, V. F. Puntes, *Mater. Sci. Eng. C* **2007**, *27*, 1236.
[30] A. M. Gobin, D. P. O'Neal, D. M. Watkins, N. J. Halas, R. A. Drezek, J. L. West, *Lasers Surg. Med.* **2005**, *37*, 123.
[31] Z. Krpetic, P. Nativo, V. See, I. A. Prior, M. Brust, M. Volk, *Nano Lett.* **2010**, *10*, 4549.
[32] M. M. Alvarez, J. T. Khoury, T. G. Schaaff, M. N. Shafigullin, I. Vezmar, R. L. Whetten, *J. Phys. Chem. B* **1997**, *101*, 3706.
[33] S. Link, M. A. El-Sayed, *J. Phys. Chem. B* **1999**, *103*, 4212.
[34] P. K. Jain, K. S. Lee, I. H. El-Sayed, M. A. El-Sayed, *J. Phys. Chem. B* **2006**, *110*, 7238.
[35] B. Palpant, Y. Guillet, M. Rashidi-Huyeh, D. Prot, *Gold Bull.* **2008**, *41*, 105.
[36] D. Lapotko, *Int. J. Heat Mass Transfer* **2009**, *52*, 1540.
[37] L. Francois, M. Mostafavi, J. Belloni, J. A. Delaire, *Phys. Chem. Chem. Phys.* **2001**, *3*, 4965.
[38] V. Kotaidis, C. Dahmen, G. v. Plessen, F. Springer, A. Plech, *J. Chem. Phys.* **2006**, *124*, 1.
[39] G. Decher, B. Lehr, K. Lowack, Y. Lvov, J. Schmitt, *Biosens. Bioelectron.* **1994**, *9*, 677.
[40] G. Decher, *Science* **1997**, *277*, 1232.
[41] A. S. Urban, A. A. Lutich, F. D. Stefani, J. Feldmann, *Nano Lett.* **2010**, *10*, 4794.
[42] W. Walcher, in *Praktikum der Physik*, 9th ed., Vieweg&Teubner, Wiesbaden, Germany **2009**.
[43] T. C. Choy, in *Effective Medium Theory: Principles and Applications*, Oxford University Press, Oxford, **1999**.
[44] E. D. Palik, in *Handbook of Optical Constants of Solids*, Academic Press, New York, **1985**.
[45] A. J. Welch, M. J. C. van Gemert, in *Optical-Thermal Response of Laser-Irradiated Tissue*, Plenum Press, New York **1995**.
[46] M. J. Guffey, N. F. Scherer, *Nano Lett.* **2010**, *10*, 4302.
[47] M. Schwagler, C. Nowak, J. Hoffmann, W. Schartl, *J. Phys. Chem. C* **2009**, *113*, 15124.
[48] M. F. Bedard, D. Braun, G. B. Sukhorukov, A. G. Skirtach, *ACS Nano* **2008**, *2*, 1807.
[49] S. T. Dubas, J. B. Schlenoff, *Macromolecules* **1999**, *32*, 8153.
[50] G. Ibarz, L. Dähne, E. Donath, H. Möhwald, *Adv. Mater.* **2001**, *13*, 1324.
[51] G. Decher, J. Schlenoff, in *Multilayer Thin Films: Sequential Assembly of Nanocomposite Materials*, 1st ed., Wiley VCH, Weinheim, **2002**.